Measurement system calibration and radiation characteristic inversion based on infrared weak and small targets

LI Wen-Xiong[1,2,3],　　SHEN Jun-Li[1,3*],　　LU Zhen-Yu[1,3],　　MEN Shu-Dong[1,3],　　WU Qing-Wen[1,3],　　ZHAO Xiao-Yan[1,3]

（1. Changchun Institute of Optics, Fine Mechanics and Physics, Chinese Academy of Sciences, Changchun 130033, China；

2. University of Chinese Academy of Sciences, Beijing 100049, China；

3. CAS Key Laboratory of On-orbit Manufacturing and Integration for Space Optics System, Changchun 130033, China）

Abstract：With the widespread application of infrared detection technology in fields such as military reconnaissance, aerospace monitoring, and security early warning, infrared measurement systems play a critical role in infrared detection. In response to issues such as low calibration efficiency and significant environmental interference in the calibration and radiative property inversion of infrared measurement systems, this paper proposes a calibration and radiative property inversion method based on infrared weak small targets. A small-area blackbody source is used as a controllable radiation source to project infrared targets, and deep learning networks are employed for precise identification and gray-scale extraction of infrared weak small targets. Using this, a calibration model for the measurement system is established. Experimental results show that the method demonstrates good calibration stability within the temperature range of 298-308 K, with the absolute error of radiative property inversion controlled within ±2 K and the relative error of inversion temperature ≤ 0. 5%. Regression analysis also indicates high temperature inversion accuracy (R^2>0. 94). Compared to traditional methods, the proposed method balances calibration efficiency and accuracy while extending the ability to invert the temperature field of targets. This research provides an effective solution for rapid calibration and high-precision radiative property analysis of infrared weak small targets.

Key words：infrared, measurement system, calibration, inversion, small targets

基于红外弱小目标的红外测量系统标定和辐射特性反演

李文雄[1,2,3]，　申军立[1,3*]，　陆振玉[1,3]，　门树东[1,3]，　吴清文[1,3]，　赵晓岩[1,3]

（1. 中国科学院长春光学精密机械与物理研究所,吉林 长春 130033；

2. 中国科学院大学,北京 100049；

3. 中国科学院空间光学系统在轨制造与集成重点试验室,吉林 长春 130033）

摘要：随着红外探测技术在军事侦察、航天监测和安防预警等领域的广泛应用,红外测量系统在红外探测技术中起着关键的作用。针对红外测量系统标定与辐射特性反演中存在的标定效率低、环境干扰大等问题,本文提出了一种基于红外弱小目标的测量系统标定及辐射特性反演方法。采用小面源黑体作为可控辐射源投射红外目标,通过深度学习网络对红外弱小目标进行精准识别与灰度提取,并以此建立测量系统标定模型。试验结果表明,该方法在 298~308 K 范围内标定稳定性良好,辐射特性反演绝对误差控制在±2 K 范围内,且反演温度相对误差≤0.5%。回归分析也表明了温度反演精度较高(R^2>0.94)。相较于传统方法,本文方法兼顾了标定效率与精度,并扩展了对目标的温度场反演能力。本研究为红外弱小目标的快速标定与高精度辐射特性分析提供了有效解决方案,在军事侦察、航天监测等领域具有应用潜力。

Introduction

Infrared detection technology plays a vital role in fields such as military reconnaissance, space surveillance, and early warning systems. It serves as one of the key means for long-range target monitoring and threat identification. With increasingly complex operational environments and diminishing target signatures, higher demands are placed on the spatial resolution, sensitivity, and response speed of infrared detection systems. However, due to the high cost of experimentation, unstable testing conditions, and the difficulty of acquiring in-situ data, traditional testing approaches are often insufficient to comprehensively evaluate system performance. To efficiently assess the operational capabilities of infrared measurement systems under conditions approximating reality, semi-physical simulation based on space simulation devices is commonly employed. This method constructs controlled infrared radiation scenes to emulate the infrared characteristics of targets, thereby enabling precise calibration and functional verification of the infrared system. Semi-physical simulation not only retains the controllability of laboratory testing, but also incorporates the dynamic characteristics of realistic operational environments, providing essential support for the reliable application of infrared measurement systems in actual missions.

Within this framework, the infrared measurement system constitutes a core component responsible for high-precision radiation detection and data acquisition. It detects infrared radiation emitted or reflected by targets and converts the signal into electrical output via signal processing units, ultimately generating gray-scale infrared images. The gray-scale distribution and its variations in these images correspond closely to the surface temperature field of the target. Calibration of infrared measurement systems serves two primary purposes: first, to establish the functional relationship between target physical quantities and image gray-scale values; and second, to correct the relative response of the system[1-2]. Accurate mapping of gray-scale values to absolute temperatures is crucial for ensuring that the images faithfully represent the thermal state of the observed object. Once calibration is complete, the system can acquire real-time image data during operation and utilize inversion algorithms to retrieve target surface temperature and radiative characteristics from the gray-scale information. These radiative features are essential for the identification, detection, and tracking of aerial targets within the system's field of view.

Wang[3] proposed an infrared radiation characteristic inversion algorithm for rotorcraft operating in small-target scenarios. By applying the inversion model at different observation angles, the distribution of infrared radiation intensity for a specific rotorcraft in the 3-5 μm band was obtained. Zhang[4] conducted radiation calibration of an uncooled long-wave infrared thermal imager using a large-area blackbody within a temperature range of 25 °C to 40 °C. The results showed that the calibrated thermal imager achieved a temperature measurement error of less than 0.5 °C. Montanaro[5] developed a radiation calibration method for the Landsat 8 thermal infrared sensor, enabling the conversion of raw instrument output into precise aperture spectral radiance. The calibration process involved detector linearization, background removal, and radiance conversion using a calibration look-up table. Lu[6] constructed a field calibration system for infrared systems, analyzing the energy transfer process, experimental procedures, system response, and the physical significance of system baseline gray-scale values for direct, indirect, and close-range calibrations using a blackbody source. Cui[7] proposed a space point-source target infrared radiation brightness inversion method for ground-based infrared imaging systems, deriving a radiation calculation model that accounts for factors such as energy diffusion, pixel signal aliasing, and focal plane array duty cycle. The inversion accuracy was found to be within 20% after ground-based standard star measurement experiments. Yang[8] and others, addressing the issue of reduced calibration accuracy in high-dynamic infrared imaging systems caused by fixed integration time and transmittance, proposed an improved calibration algorithm that considers integration time and transmittance. Experiments demonstrated that the calibration accuracy of the proposed algorithm could reach around 1%. Lin[9] introduced a novel radiation calibration method designed to mitigate errors caused by environmental temperature drift and internal heating. The method employed multivariate and second-order polynomials to correct thermal imager outputs and utilized a Planck-like approximation function to calculate object temperature from thermal image gray-scale values. Experimental validation showed that this method achieved high calibration accuracy.

Most existing studies still primarily rely on laboratory large-area blackbodies or field target imaging for calibration. Large-area blackbodies, owing to their extensive surface areas, can provide a highly uniform radiation field over a wide region and maintain stable surface temperatures due to their large thermal capacity. However, their substantial size results in slow heating and cooling rates, and the associated equipment is bulky, making them unsuitable for rapid and high-frequency calibration tasks. In contrast, field target imaging calibration is more suitable for rapid and frequent calibration; however, the complex outdoor environment, including atmospheric effects, solar radiation, and ground background interference, can significantly degrade calibration accuracy. Both types of existing calibration methods exhibit limitations in practical applications, struggling to simul-

2 期

LI Wen-Xiong *et al*：Measurement system calibration and radiation characteristic inversion based on infrared
weak and small targets

343

taneously balance flexibility, precision, and efficiency.

To address these shortcomings, this study proposes a novel method for calibrating infrared measurement systems and inverting radiation characteristics based on weak and small infrared targets. The method employs a small-area blackbody with good thermal responsiveness to provide a stable and controllable infrared radiation source. Owing to its excellent radiation uniformity and adjustable temperature characteristics, the small-area blackbody can simulate infrared radiation fields under various actual working conditions. During the system calibration phase, an infrared target detection algorithm is first applied to accurately identify small infrared targets. Subsequently, the temperature, image gray-level, and radiance of the infrared radiation source are precisely measured and calculated, providing reliable data support for subsequent radiation characteristic inversion. After completing system calibration, based on the obtained calibration results, the radiation characteristics of the target —including surface temperature, radiance, temperature field distribution, and other surface properties—are inversely solved using the image gray-level information.

The proposed method ensures calibration accuracy while simultaneously offering rapidity and adaptability to complex environments. It effectively enhances the overall performance of infrared measurement systems in weak and small target detection, complex scene adaptability, and dynamic response capabilities. Through the combined use of small-area blackbodies and infrared target detection algorithms, the limitations of traditional methods are overcome, providing crucial support for extending the applications of infrared detection devices in fields such as precision measurement, dynamic monitoring, and efficient calibration.

1　Infrared weak and small target detection

In the calibration and radiation characteristic inversion of infrared weak and small target measurement systems, the first critical step is the identification and detection of infrared small targets. Compared to general detection tasks, detecting infrared small targets presents significant challenges due to their weak energy, small sizes, and their tendency to be submerged within noise and cluttered backgrounds. Moreover, the signal characteristics of small targets are typically ambiguous, resulting in low contrast between the target and the surrounding background[10]. Consequently, enhancing the prominence of target signals, suppressing background interference, and improving detection robustness have become core challenges in the field of infrared small target detection[11].

Traditional methods for infrared small target detection often rely on low-rank and sparse decomposition models. By isolating sparse components, these approaches effectively suppress background noise and enhance the prominence of target signals, thereby facilitating the detection and identification of infrared small targets[12-13]. However, recent advances in deep learning technologies have demonstrated significant advantages and broad ap-

plication prospects in this field. Compared to traditional methods, deep learning models can automatically extract features from data by constructing end-to-end frameworks, exhibiting strong adaptability, particularly in scenarios characterized by weak target features, small target sizes, and complex backgrounds. Common deep learning architectures used for infrared target detection include convolutional neural network（CNN）, U-Net, and YOLO [14-16]. These models achieve deep feature extraction through multi-layer network structures. Moreover, with the support of large-scale labeled datasets, deep learning approaches substantially enhance robustness under low signal-to-noise ratio（SNR）conditions and enable collaborative optimization of target detection and background suppression via multi-task learning strategies. Despite these advancements, challenges remain, including insufficient labeled training data, high computational complexity, and limited generalization capability in real-world scenarios.

Based on the preceding analysis and discussion, although deep learning exhibits certain limitations in infrared small target detection, it remains a powerful and promising approach in this field. In this study, a U-Net-based model, termed ISTDU-Net[17], is employed for infrared small target detection. ISTDU-Net is a U-shaped deep learning architecture that transforms a single-frame infrared image into a probability likelihood map highlighting the presence of small targets. To enhance small target representation, ISTDU-Net introduces feature map grouping and amplifies the weights of small target-related feature groups during network down-sampling. Additionally, fully connected layers are incorporated into the skip connections, enabling the model to suppress extensive background regions with similar structures by leveraging the global receptive field, thereby improving the contrast between targets and background.

The indirect blackbody calibration method is used, and the target is identified and detected through ISTDU-Net. The experimental setup is shown in Fig. 1. The experiment primarily includes a simulated target blackbody, a collimated optical system, and a measurement system. Measurement system parameters are shown in Table 1. Based on the resolution and pixel pitch of the measurement system, a target occupying fewer than 20 pixels in the image is considered a small target. Therefore, to simulate infrared small targets, the blackbody temperature is set close to the ambient temperature, and the radiation is emitted outward through a 1 mm pinhole. After passing through the pinhole, the radiation from the simulated blackbody target is directed into the measurement system's focal plane via a collimated optical system, where it is detected by the infrared sensor. The measurement system captured gray-scale images of the pinhole, which are then processed using ISTDU-Net for recognition and detection. Targets located within the detection boxes output by ISTDU-Net are identified as the infrared small targets detected by the network.

In the experiment, data are collected and recorded multiple times within the range of 298 K to 308 K with a
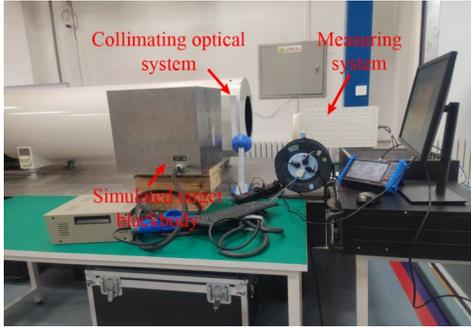
Fig. 1　Experimental setup
图1　试验布置

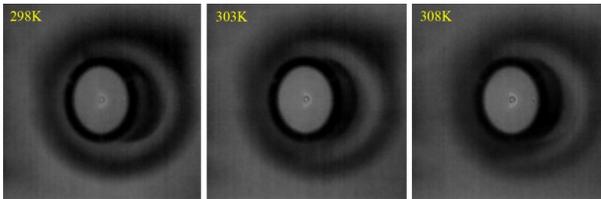1 K gradient, and some of the results are shown in Fig. 2.

Fig. 2　Simulated target gray-scale image
图2　模拟目标灰度图像

The calibration experiment yielded multiple sets of experimental data. The ISTDU-Net infrared small target detection method is applied to detect the measured pinhole gray-scale images. Figure 3 shows the results of IST-DU-Net applied to the 1 mm pinhole gray-scale images captured by the measurement system, with corresponding infrared small targets at blackbody temperatures of 298 K, 303 K, and 308 K. The left side of Fig. 3 shows the detection results of ISTDU-Net for the pinhole, where the position and pixel count of the pinhole are identified. The right side of Fig. 3 shows the gray-scale distribution map of the measurement system's gray-scale image. This process successfully simulates, recognizes, and extracts information from infrared small targets. Based on this experimental data, the calibration task of the measurement system for the target is completed.

Table 1　Measurement system parameters
表1　测量系统参数

Parameters	Value
Detector Type	Infrared FPA
Resolution	640×512
F−Number	1.0
Pixel Pitch	12 μm
Response Wavelength	8−14 μm

2　Measurement system calibration

This paper uses ISTDU-Net to detect infrared small targets by a certain camera and obtain the gray-scale values of each pixel of the target. Based on the gray-scale values, the measurement system is calibrated and radiation characteristics are inverted. The gray-scale mean, which is the average gray-scale value of all pixels in the image, is introduced. Let the infrared target to be analyzed by $f(x, y) \in \mathbb{R}^{m \times n}$,
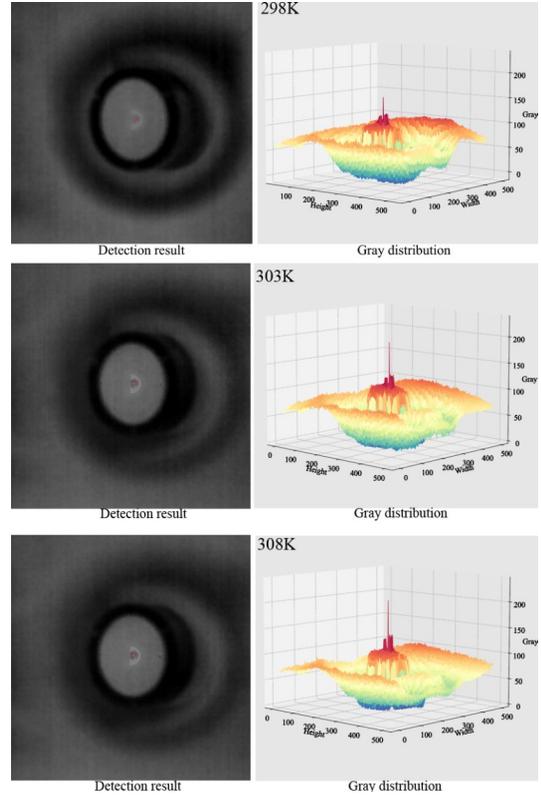

Fig. 3　Detection results and gray-scale distribution
图3　探测结果和灰度分布

where x and y are the row and column indices of the target, and m and n are the height and width of the target, respectively. The gray-scale mean is defined as shown in Eq. 1. Generally, the larger the gray-scale mean μ, the higher the overall gray-scale value of the target. The average gray-scale value of each pixel in the infrared small target detected by the network is used as the calibration parameter for the measurement system.

$$\mu = \frac{1}{m \times n} \sum_{i=1}^{m} \sum_{j=1}^{n} f(i,j) \qquad . \quad (1)$$

The infrared target radiation measurement model can generally be expressed as $DN = K(\tau_\alpha L_t + L_{path}) + B$, where DN is the gray-scale value corresponding to the target in the infrared measurement system, τ_α is the atmospheric transmittance, L_{path} is the atmospheric path radiance, L_t is the target radiance, K is the system's radiance response, and B is the gray-scale offset.

The measurement system in this study is primarily used in a vacuum simulation device for semi-physical simulation tasks. The impact of atmospheric factors is not considered. Therefore, the model can be simplified to $DN = KL_t + B$. During the calibration process, the blackbody temperature is known, and according to

Planck's Law (Eq. 2), the radiance L_t is known. T is the blackbody temperature, λ is the wavelength, $c_1 \approx 3.74 \times 10^{-16}$ J/K is the first radiation constant, and $c_1 \approx 1.44 \times 10^{-2}$ m·K is the second radiation constant.

$$L_t(T) = \frac{1}{\pi} \int_{\lambda_1}^{\lambda_2} \frac{c_1}{\lambda^5} \frac{\mathrm{d}\lambda}{e^{\left(\frac{c_2}{\lambda T}\right)} - 1} \qquad . \quad (2)$$

Through blackbody calibration experiments, multiple sets of gray-scale images and corresponding simulated target blackbody temperatures are obtained, forming the DN-T data for system calibration. Here, DN represents the gray-scale mean, which is the average gray-scale value of all pixels of the infrared small target detected by ISTDU-Net. T is the simulated target blackbody temperature, used to calculate the corresponding radiance of the simulated target. Using this data, the relationship between radiance L and gray-scale mean DN is established, as shown in Eq. 3. The system's radiance response K and gray-scale offset B within this temperature range are then solved using the least squares fitting method.

$$\begin{cases} DN_1 = K \frac{1}{\pi} \int_{\lambda_1}^{\lambda_2} \frac{c_1}{\lambda^5} \frac{\mathrm{d}\lambda}{e^{\left(\frac{c_2}{\lambda T_1}\right)} - 1} + B \\ DN_2 = K \frac{1}{\pi} \int_{\lambda_1}^{\lambda_2} \frac{c_1}{\lambda^5} \frac{\mathrm{d}\lambda}{e^{\left(\frac{c_2}{\lambda T_2}\right)} - 1} + B \\ \cdots \\ DN_n = K \frac{1}{\pi} \int_{\lambda_1}^{\lambda_2} \frac{c_1}{\lambda^5} \frac{\mathrm{d}\lambda}{e^{\left(\frac{c_2}{\lambda T_2}\right)} - 1} + B \end{cases} \quad . \quad (3)$$

Three sets of temperature measurements, each with three different temperatures, are selected from the experimental data for the radiation calibration of the measurement system. The results obtained through the least squares fitting method are shown in Table 2 and Fig. 4.
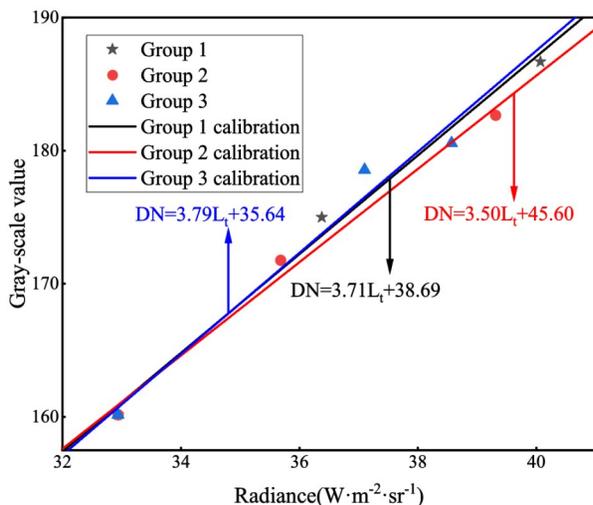

Fig. 4   Calibration curve
图 4   标定曲线

In Table 2, the temperature, gray-scale mean, system radiance response, and gray-scale offset for the three sets of calibration data are described. Figure 4 shows the

Table 2   Calibration results
表 2   标定结果

Group	Temperature (K)	Gray-scale mean value	System radiance response	Gray-scale migration
1	298.15	160.17		
	303.15	175.00	3.71	38.69
	308.15	186.67		
2	298.15	160.17		
	302.15	171.78	3.50	45.60
	307.15	182.67		
3	298.15	160.17		
	304.15	178.56	3.79	35.64
	306.15	180.56		

distribution of the three sets of calibration data and the calibration curve model obtained through the least squares fitting method. From Table 2 and Fig. 4, it can be concluded that by using ISTDU-Net for infrared small target recognition and implementing radiation calibration of the measurement system based on the gray-scale mean, the calibration results for the three sets of different data are consistent within the target range, demonstrating good calibration stability. In subsequent work, the calibration model obtained will be used for radiation characteristic inversion of the target. It is important to note that, without calibration, the measurement system is limited to capturing the gray-scale information of the target, with no established mapping to radiance (or temperature), thereby preventing radiation characteristic inversion. The proposed calibration method enables the development of an accurate radiometric response model, which is essential for the subsequent inversion of the target's radiation characteristics.

3   Radiation characteristic inversion

After completing the radiation calibration of the measurement system, the infrared radiation measurement model $DN = KL_t + B$ for the measurement system itself is obtained. For unknown target gray-scale images, the inverse solution is performed following the above calibration process, enabling the inversion of the target's radiation characteristics. The target gray-scale image is detected using ISTDU-Net, and the corresponding number of pixels and gray-scale values of the target are extracted. Then, radiation brightness inversion is performed based on Eq. 4. The target temperature is then inverted using a numerical method. Equation 3 is used to construct Eq. 5, which is solved using the Newton-Raphson method to obtain the target temperature.

$$L_t(T) = \frac{DN - B}{K} \qquad , \quad (4)$$

$$f(T) = \frac{1}{\pi} \int_{\lambda_1}^{\lambda_2} \frac{c_1}{\lambda^5} \frac{\mathrm{d}\lambda}{e^{\frac{c_2}{\lambda T}} - 1} - L_t \qquad . \quad (5)$$

Based on the above method, the three calibration models obtained are used to invert the temperature range from 298 K to 308 K. The inversion results for each
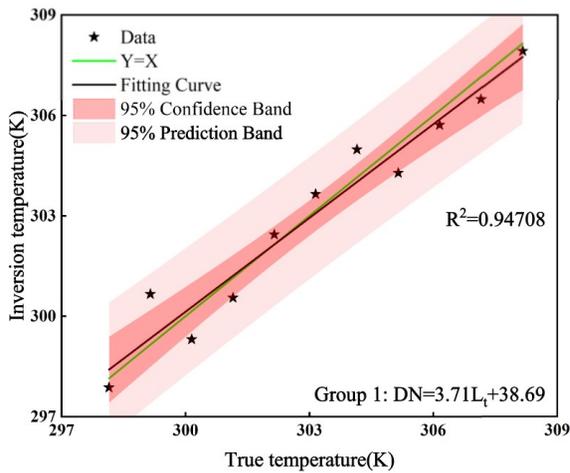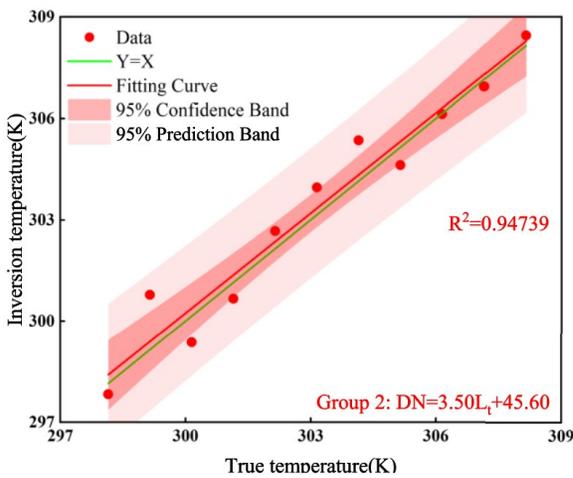
Fig. 5　Group 1 regression analysis
图5　标定组1回归分析

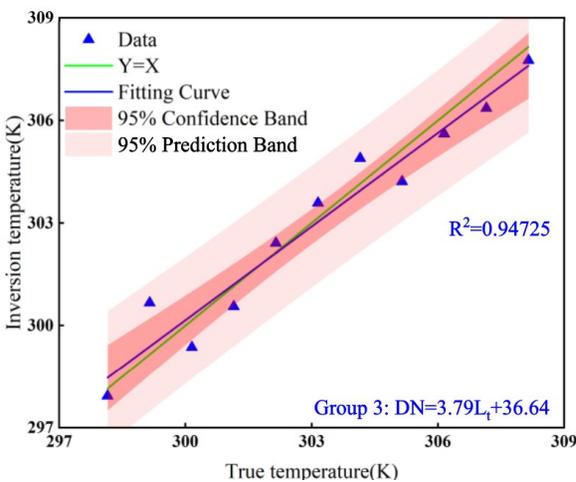Fig. 6　Group 2 regression analysis
图6　标定组2回归分析

Fig. 7　Group 3 regression analysis
图7　标定组3回归分析

group are shown in Tables 3-5. From the tables，it can be concluded that each group of models achieves high inversion accuracy. The inversion errors are all controlled

within ±2 K，and the relative errors are all ≤0. 5%. The regression analysis results are shown in Figs. 5~7.

Table 3　Group 1 inversion results
表3　标定组1反演结果

	True temperature	Inversion temperature	Absolute error	Relative error
	298. 15	297. 87	−0. 28	−0. 09%
	299. 15	300. 66	1. 51	0. 50%
	300. 15	299. 31	−0. 84	−0. 28%
	301. 15	300. 55	−0. 60	−0. 19%
	302. 15	302. 44	0. 29	0. 09%
Group1	303. 15	303. 65	0. 50	0. 16%
	304. 15	304. 98	0. 83	0. 27%
	305. 15	304. 28	−0. 87	−0. 28%
	306. 15	305. 71	−0. 44	−0. 14%
	307. 15	306. 48	−0. 67	−0. 22%
	308. 15	307. 92	−0. 23	−0. 07%

In Figs. 5~7，the x-axis represents the true temperature，and the y-axis represents the inverted temperature. The R^2 values for all three models are greater than 0. 94，indicating a good fit between the true temperature and the inverted temperature，with the models demonstrating good inversion results.

To expand the application scenarios of the method presented in this paper，temperature field inversion is performed for simulated target temperatures of 300 K，303 K，and 306 K within the temperature range. As shown in Fig. 8，the central region（crescent-shaped）of the gray-scale image captured by the measurement system is used for temperature field inversion. First，the central region of the image is selected，and the gray-scale values of all the pixels within that region are read.

Table 4　Group 2 inversion results
表4　标定组2反演结果

	True temperature	Inversion temperature	Absolute error	Relative error
	298. 15	297. 87	−0. 32	−0. 11%
	299. 15	300. 66	1. 63	0. 54%
	300. 15	299. 31	−0. 78	−0. 26%
	301. 15	300. 55	−0. 48	−0. 16%
	302. 15	302. 44	0. 52	0. 17%
Group2	303. 15	303. 65	0. 81	0. 27%
	304. 15	304. 98	1. 20	0. 39%
	305. 15	304. 28	−0. 53	−0. 17%
	306. 15	305. 71	−0. 02	−0. 01%
	307. 15	306. 48	−0. 21	−0. 07%
	308. 15	307. 92	0. 30	0. 09%

Then，the gray-scale value sequence of the central region is input into the previously obtained measurement system calibration model. Finally，the inverted tempera-

ture field data for the central region is visualized，with the results shown on the right side of Fig. 8. Therefore，the method in this paper can not only perform temperature inversion for infrared small targets but also for large or surface targets，demonstrating a broad range of application scenarios.

Table 5 Group 3 inversion results
表5 标定组3反演结果

	True temperature	Inversion temperature	Absolute error	Relative error
	298. 15	297. 93	−0. 22	−0. 07%
	299. 15	300. 67	1. 52	0. 51%
	300. 15	299. 36	−0. 79	−0. 26%
	301. 15	300. 56	−0. 59	−0. 19%
	302. 15	302. 41	0. 26	0. 09%
Group3	303. 15	303. 59	0. 44	0. 15%
	304. 15	304. 89	0. 74	0. 24%
	305. 15	304. 21	−0. 94	−0. 31%
	306. 15	305. 61	−0. 54	−0. 18%
	307. 15	306. 36	−0. 79	−0. 26%
	308. 15	307. 76	−0. 39	−0. 13%

4 Conclusion

This paper proposes a method for measurement system calibration and radiation characteristic inversion based on infrared small targets. First，an experimental setup simulating infrared small targets was constructed，and corresponding experimental data were collected. Based on these data，the ISTDU-Net algorithm was employed to detect the gray-scale images of the simulated blackbody targets，enabling accurate extraction of target pixel counts and their corresponding gray-scale values. By combining the calibration model of the measurement system with the experimental results，the system's radiance response characteristics and gray-scale offsets within a specific temperature range were obtained，thus completing the calibration process. Based on different sets of experimental data，three DN-L models for the measurement system were established.

These radiation models were then used to invert the radiation characteristics of blackbody targets at various temperatures within the experimental range. The results show that the inversion errors were controlled within ±2 K，demonstrating that the proposed method achieves high inversion accuracy. To further expand the application scenarios，temperature field inversion was also performed on target gray-scale images，and the results demonstrated good performance in reconstructing the temperature fields.

Although the proposed method achieves high accuracy in the temperature or temperature field inversion of small targets，certain limitations remain. Currently，the method is mainly applicable to static or low-speed moving targets，and challenges persist in accurately calibrating and inverting the radiation characteristics of high-
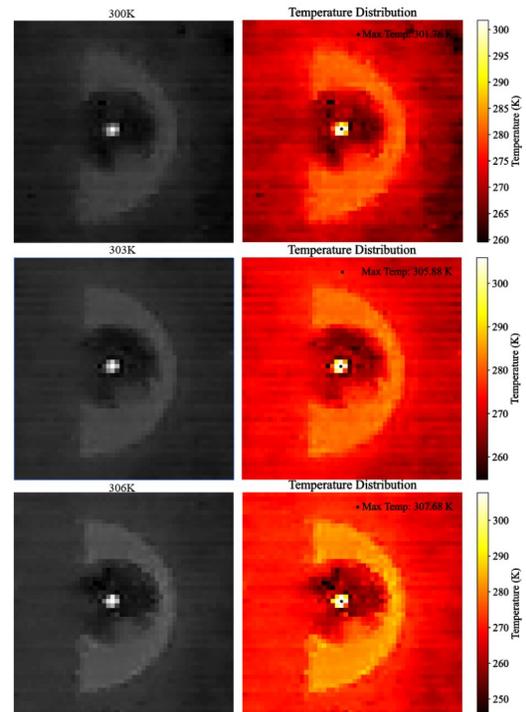

Fig. 8 Temperature field distribution
图8 温度场分布

speed moving targets. Future research will focus on the calibration and radiation characteristic inversion of measurement systems for high-speed flying targets to further enhance the applicability and precision of the proposed method. In subsequent research，we plan to integrate field test data to further assess and validate the performance of the proposed method in real-world environments，thereby ensuring its reliability and practicality in actual applications. The accumulation of field test data will be a key focus of our future work，and we aim to provide more comprehensive validation of the method through these data，ultimately enhancing its practical applicability.

References

[1] Wu C Q, Qi C L, Hu X Q, et al. FY−3D HIRAS radiometric calibration and accuracy assessment[J]. IEEE Transactions on Geoscience and Remote Sensing, 2020, 58(6): 3965−3976.

[2] Gan S Q, Wang W C, Yuan G F, et al. Computation model for calculating infrared radiance of aerial target based on each pixel calibration of refrigeration infrared system[J]. Acta Optica Sinica, 2024, 44 (12): 1212001.

[3] Wang B, Gao Q, Zhang Y X. Characterization and inversion method of infrared radiation properties of helicopter in point source detection [J]. Infrared, 2018, 39(05): 37−41.

[4] Zhang X L, Liu Y, Sun Q. Radiometric calibration of uncooled long−wave infrared thermal imager with high−precision [J]. Chinese Optics, 2012, 05(03): 235−241.

[5] Montanato M, Lunsford A, Tesfaye Z, et al. Radiometric calibration methodology of the Landsat 8 thermal infrared sensor [J]. Remote Sensing, 2014, 6: 8803−8821.

[6] Lu X F, Sheng J, Zhao H. Outdoor calibration system of infrared device and method of computing luminance of aircraft [J]. Infrared Technology, 2015, 37(02): 154−160.

[7] Cui W Y, Chen C, Yi W. Radiation characteristic inversion of space point source target based on infrared imagery [J]. SPIE, 2015, 9674: 96742Y.

［8］Yang G Q, Yu Y, Sun X Y, et al. Radiometric calibration algorithm for high dynamic range infrared imaging system［J］. Infrared Physics & Technology, 2023, 130: 104607.

［9］Lin D, Cui X J, Wang Y, et al. Pixel-wise radiometric calibration approach for infrared focal plane arrays using multivariate polynomial correction［J］. Infrared Physics & Technology, 2022, 123: 104110.

［10］Xue W, Qi J H, Shao G Q, et al. Low-rank approximation and multiple sparse constraint modeling for infrared low-flying fixed-wing UAV detection［J］. IEEE Journal of Selected Topics in Applied Earth Observations and Remote Sensing, 2021, 14: 4150-4166.

［11］Wang X Y. Research on infrared dim and small target detection theory and methodology based on sparse dynamic inversion［D］. University of Electronic Science and Technology, Sichuan, 2018.

［12］Zhang L, Peng Z. Infrared small target detection based on partial sum of the tensor nuclear norm［J］. Remote Sensing, 2019, 11(4): 382-415.

［13］Gao C Q, Meng D Y, Yang Y, et al. Infrared patch-image model for small target detection in a single image［J］. IEEE Transactions on Image Processing, 2013, 22(12): 4996-5009.

［14］Fan M M, Tian S Q, Liu K, et al. Infrared small target detection based on region proposal and CNN classifier［J］. Signal, Image and Video Processing, 2021, 15: 1927-1936.

［15］Tong X Z, Sun B, Wei J Y, et al. EAAU-Net: enhanced asymmetric attention U-Net for infrared small target detection［J］. Remote Sensing, 2021, 13(16): 3200.

［16］Hao X Y, Luo S J, Chen M Y, et al. Infrared small target detection with super-resolution and YOLO［J］. Optics & Laser Technology, 2024, 177: 111221.

［17］Hou Q Y, Zhang L W, Tan F J, et al. ISTDU-Net: infrared small-target detection U-Net［J］. IEEE Geoscience and Remote Sensing Letters, 2022, 19: 7506205.